Origin of the complex dielectric relaxation spectra of molecular glass formers

F. J. Bermejo,[1,2] W. S. Howells,[3] M. Jiménez-Ruiz,[4] M. A. González,[4] D. L. Price,[5,6] M. L. Saboungi,[7,6] and C. Cabrillo[2]
[1]*Department of Electricity and Electronics, University of Basque Country, P.O. Box 644, Bilbao 48080, Spain*
[2]*Instituto de Estructura de la Materia, Consejo Superior de Investigaciones Científicas, Serrano 123, E-28006 Madrid, Spain*
[3]*ISIS Facility, Rutherford Appleton Laboratory, Chilton, Didcot, Oxon OX11 0QX, United Kingdom*
[4]*Institut Laue Langevin, Boîte Postale 156x, F-38042 Grenoble Cedex 9, France*
[5]*Centre de Recherches sur les Matériaux à Haute Temperature, CNRS, Orléans, France*
[6]*Argonne National Laboratory, Argonne, Illinois 60439, USA*
[7]*Centre de Recherches sur le Matière Divisée, Universitè d'Orlèans-CNRS, 45071 Orléans Cedex 2, France*
(Received 7 January 2004; published 3 May 2004)

The origin of the three broad bands appearing in the dielectric spectra of molecular glass formers is tracked down to microscopic scales by means of neutron-scattering and molecular-dynamics simulations. Three distinct regimes are also seen in the neutron quasielastic spectrum and are shown to arise from well-separated time regions appearing in the single-particle dipole autocorrelation function derived from simulations.

DOI: 10.1103/PhysRevB.69.174201 PACS number(s): 67.20.+k, 61.12.−q, 61.20.Ja

I. INTRODUCTION

The complex dielectric permittivity $\epsilon(\omega)=\epsilon'(\omega)-i\epsilon''(\omega)$ of most molecular glass formers usually spans ten frequency decades or so and shows a few low-frequency bands. The peak frequencies appearing in $\epsilon''(\omega)$ show strong temperature dependencies, particularly as one crosses the melting temperature and enters the supercooled liquid (SCL) range. The microscopic origin of such relaxations is still a matter of discussion.[1–7] In particular, the issue of whether different bands should be associated with well-defined physical processes has been debated in the literature for quite some time.[1,2,6,7] A firm understanding of the origin of these macroscopic relaxations would then provide a sound basis for studying the liquid dynamics at temperatures close to T_g, the temperature that signals the liquid→glass transition where the usual diffusion approximations employed for the analysis of normal-liquid data are suspected to break down (see Frölich in Ref. 1).

Some small-chain alcohols are particularly advantageous samples to employ because of the long lifetimes of their SCL states as well as the simplicity of their molecular structures which makes them amenable to atomistic simulations using realistic interaction potentials. Their lowest-frequency relaxations which take most of the spectral power usually show a deceptively simple shape (i.e., Lorentzian or Debye-like) which is the expected behavior for the isotropic, high-temperature reorientations of individual dipoles. Higher-frequency bands appear either as well-defined peaks or shoulders[6] whose nature is also a matter of debate.[3,6]

Here we report on the dynamics of 1-propanol as explored by the combined use of quasielastic neutron-scattering (QENS), dielectric relaxation,[3] and computer molecular-dynamics simulations. Our point of departure is to exploit the information provided by QENS on the spatial dependence of microscopic motions that allows us to assign them mass-diffusion or rotational characters. In addition, molecular dynamics (MD) enables us to access quantities hardly amenable to experiment such as information about the motions of molecular centers of mass, individual dipole reorientations, or measures of rotation-translation coupling.

The SCL range for this sample spans from $T_g=98$ K up to melting at $T_m=148$ K. Its crystal and glass structures have recently been determined.[8] In addition, the specific heats for glass and crystals at temperatures both low and about T_g (Ref. 9) have recently been measured and interpreted within the framework of the soft-potential model. Last but not least, the generalized frequency spectra have been determined by experimental means, and the assignment of its most prominent features has been carried out with the aid of MD simulations.[10]

In what follows we establish some common features for motions probed by different experimental and simulational techniques. Measurements of the quasielastic line broadening in neutron-scattering experiments constitute our starting point. The choice of such a technique as our main source of experimental data stands for the relative ease of interpretation of neutron data which may be analyzed following a Bayesian approach that only involves rather general assumptions about the general form of the relaxation functions.

Dielectric relaxation data are then measured over a comparable range of temperatures. The broad frequency distributions are described in terms of a few parameters that will later be compared to those derived from QENS. The origin of the three different relaxations seen by QENS and dielectric spectroscopy are then tracked down to microscopics with the aid of results from molecular simulations.

II. EXPERIMENT

A. Quasielastic neutron scattering

The QENS measurements provide dynamic structure factors $S(Q,\omega)$ that are dominated by incoherent scattering from molecular protons. The spectral frequency distribution determined in previous works[10] comprises a region of stochastic and intermolecular vibrations that extend over a frequency range up to some 9 THz. We thus expect the lower-frequency part of such a region to exhibit a strong temperature dependence that will mimic the behavior of the

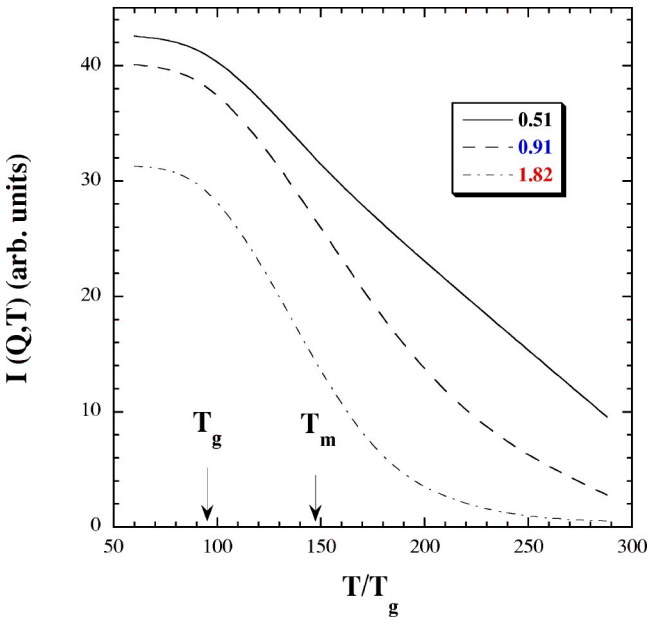

FIG. 1. Fixed-window measurement using the IRIS spectrometer for three values of the momentum transfer as indicated in the inset.

macroscopic transport coefficients for mass and angular momentum. Such parallelism is usually limited to temperatures well above melting due to the intricacy of molecular motions.

A suite of three different spectrometers is employed here to cover a wide range of energy transfers with high resolution. The two backscattering spectrometers IN10 (ILL, Grenoble, France) and IRIS (ISIS, UK) provided energy resolutions (half-width at half maximum) of about $\Delta E \approx 0.12$ GHz and $\Delta E \approx 2.05$ GHz, respectively, allowing us to explore energy transfers of -3.6 GHz$<E<3.6$ GHz and -0.1 THz$<E<0.1$ THz, respectively. A wider frequency window was also explored with the IN6 time-of-flight spectrometer at the ILL.

A preliminary study of the transfer of intensity from the unresolved (or elastic) line into the quasielastic wings was carried out on IRIS by means of a fixed-window measurement that monitors the transfer of intensity outside the energy window referred to above. Figure 1 shows how a strong drop of the elastic intensity starts to develop at temperatures just above T_g and most of the spectral intensity gets out of the IRIS instrument window at room temperature for the larger momentum transfers.

Unbiased estimates for the QENS spectral parameters (linewidths and amplitudes) are derived from line-shape analysis following a Bayesian approach.[12] The procedure which has proven to be very useful in situations where the number of parameters to be optimized is not known provides an answer to the question. Given that the quasielastic spectrum consists of a few components, how many of those are most evident in the data and what are their linewidths and amplitudes?[12] The rationale behind such method stems from Bayes' theorem that relates the conditional probability distribution function prob$[S|D,I]$ that summarizes our inference about the spectrum S, given the data S and our previous knowledge I to

$$\text{prob}[S|D,I] \propto \text{prob}[D|F,I]\text{prob}[F|I], \tag{1}$$

which is a quantity we can calculate, prob$[D|F,I]$, and another which encodes the previous knowledge (i.e., positivity of the spectrum, its normalization, etc.), prob$[F|I]$. The latter are referred to as the *prior* probability distribution function and codifies our state of knowledge (or the lack of it) about the sought spectrum. Such prior distribution is then modified by the data through the likelihood function prob$[D|F,I]$ and from the product of both one gets the *posterior* distribution that represents our knowledge about S after we have analyzed the data.

As a prior distribution we employ a single Lorentzian line with a linewidth calculated from the values of the self-diffusion coefficient as measured by pulsed field-gradient NMR.[11] The linewidth $\Delta\omega_i$ and line strengths A_i are then refined together with estimates for parameters defining the other spectral components. The procedure involves an analysis of the quality of the fits assuming the presence of 0–3 quasielastic lines. We found that for temperatures above T_g (150 K$<T<$290 K) the spectrum is composed of three Lorentzians. A sample of the spectral parameters corresponding to the two narrower lines is shown in Fig. 2.

Above $\approx$230 K the Q dependence of $\Delta\omega_i$ for the narrowest peak follows the $D_T Q^2$ Fick's law with D_T being the translational diffusion coefficient, while the amplitudes fulfill $A_i \propto 1/D_T Q^2$, which constitute clear signatures of long-range translational diffusion. The linewidths and amplitudes of the wider peaks point towards rotational processes. Their $\Delta\omega$'s comprise a translational and a Q-independent rotational component specified by a rotational constant D_R, having an amplitude that increases with wave vectors and temperature. The quasielastic spectra measured at temperatures within the deeply SCL are dominated by a single quasielastic-broadened line that shows a noticeable Q dependence. In contrast with the behavior at high temperature, the linewidths shown for $T=120$ K do not go to 0 at low Q and their amplitude decays by about 50% within the explored Q range. This is interpreted as a signature of a rotational excitation with a linewidth comprising a rotational diffusion, Q-independent term plus an effective Q^2 term D_T^{eff} which appears as a result of higher-order contributions. As we will see below this effective term comprises faster motions than those attributable to mass diffusion, and therefore it is assigned to a translation-rotation process.

B. Dielectric spectroscopy

The dielectric spectra comprising a frequency interval 10^{-1} Hz$<\omega<10^9$ Hz[3] also show a minimum of three distinct features. An example of the measured data is given in Fig. 3. $\epsilon(\omega,T)$ are well fitted by a Debye plus a Cole-Davidson function to account for the two low-frequency processes plus a log-normal distribution for the highest-frequency relaxation. Such a model reads

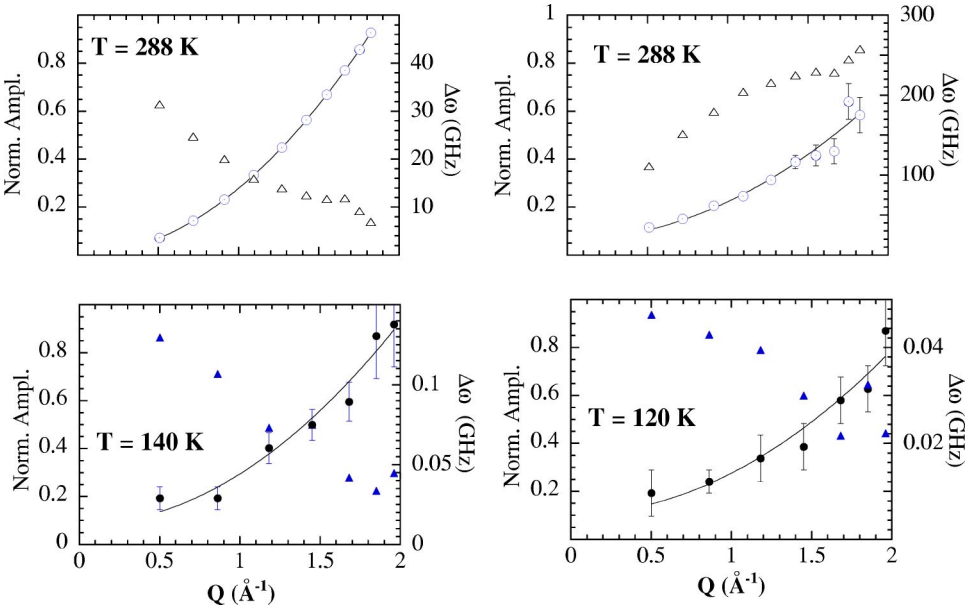

FIG. 2. The upper frames show the quasielastic linewidths (circles with a dot) and fractional amplitudes (open triangles) for the two narrowest lines of the normal liquid. Solid lines are fits to diffusion approximations (see below). The lower two frames depict the linewidth (circles) and amplitude (triangles) of the narrowest line for two temperatures within the SCL.

$$\epsilon = \epsilon_\infty + \sum_{i=1}^{2} \frac{\epsilon_{0i} - \epsilon_{\infty i}}{(1 - i\omega/\omega_{pi})^{\alpha_i}} + i \frac{\epsilon_{03} - \epsilon_{\infty 3}}{\sqrt{\pi} W} e^{-[\ln f - \ln f_{p3}]^2/W^2}, \tag{2}$$

where $\epsilon_{0i} - \epsilon_{\infty i}$ are static susceptibility strengths, ω_{pi} the peak frequencies (relaxation times are $\tau_i \propto \omega_{pi}^{-1}$), $\epsilon_{\infty i}$ the permittivity at high frequencies, α_i is the width parameter which usually varies between 0 and 1 ($\alpha_i = 1$ for exponential relaxation), and f_{p3} and W are the $1/e$ peak frequency and half-width of the highest-frequency peak.

The main peak shows a Lorentzian shape ($\alpha_1 = 1$) that extends over a decade in frequency above its maximum. The temperature dependence of its relaxation times follows the Vogel-Fulcher-Tamman (VFT) law yielding an activation energy of 1510 K that is 1.3 times that of the shear viscosity, an attempt frequency (i.e., preexponential factor) of 0.17 THz that becomes comparable with the translational quasielastic linewidths at high temperature, and an effective temperature $T_0 = 54$ K. A higher-frequency ''shoulder'' or secondary relaxation showing a nonexponential shape and an amplitude one order of magnitude weaker than that of the main peak appears about two frequency decades above the main peak. Its shape is well accounted for by a Cole-Davidson function with an exponent $\alpha_2 \approx 0.3$. Its relaxation times also follow a VFT law with activation energy of 1410 K, $T_0 = 60$ K, and an attempt frequency of 7.8 THz that suggests that the motions here being sampled should have a dominant reorientational character. Finally, a high-frequency or β relaxation two orders of magnitude weaker than the main peak appears within 2–4 frequency decades above the secondary.

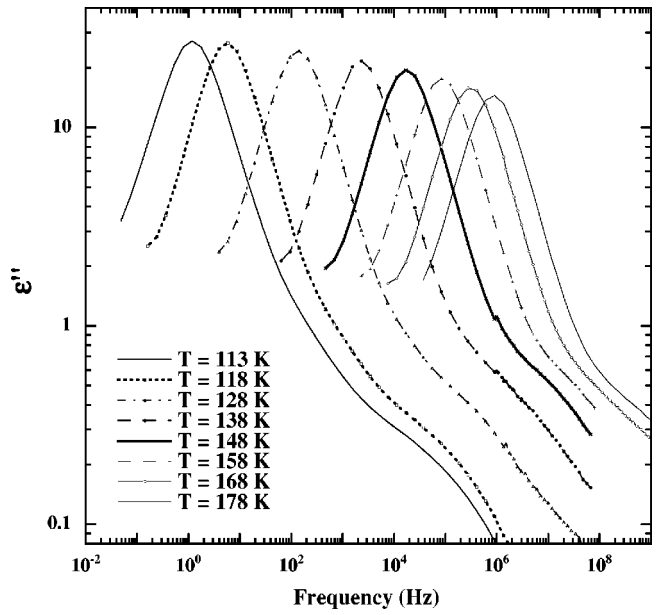

FIG. 3. A sample of the dissipative part of the measured data for temperatures given in the inset.

III. COMPUTER SIMULATION

As a source of information on some quantities not directly amenable to experiment, we have carried out a set of molecular-dynamics computations using transferable interaction potentials following steps analogous to those taken for other alcohols.[10] The quantities we will first consider are the orientational correlation functions $C_1(t) = \langle P_1(\cos\theta) \rangle$, where P_1 stands for a Legendre polynomial for an angle subtended by the molecular dipole moment vector μ and a molecular reference frame.

The main result shown in Fig. 4 concerns the presence within the first nanosecond of $C_1(t)$ of three distinct regimes. Below ≈ 0.5 ps $C_1(t)$ has an oscillatory structure that gives rise to finite-frequency peaks in spectra for energy transfers about 9 THz, as confirmed by experiment as well as by explicit calculation of the full frequency spectrum.[10] Within this time range the relaxations are well fitted by a damped cosine function[13] such as that employed in vibrational spectroscopy. Between ≈ 1 ps and ≈ 10–20 ps, a strong temperature-dependent drop is seen showing a shape

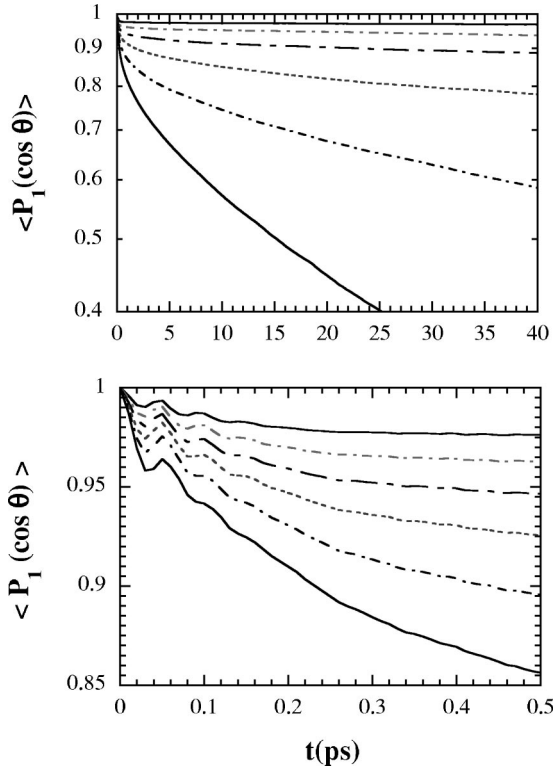

FIG. 4. The upper frame shows the intermediate to long and the lower frame depicts the short-time behaviors of $C_1(t)$ for $T=97$ K, 137 K, 176 K, 214 K, 254 K, and 290 K (from top to bottom).

that can be very well approximated by a Cole-Davidson function expressed in time domain.[14] Finally, a region of apparently exponential relaxation is attained above 10–20 ps (depending upon temperature).

Motions corresponding to the long-time region of $C_1(t)$ are of diffusive nature and give rise to quasielastic components discussed above. These reorientational motions are highly anisotropic, as judged by calculation of $C(t)$ for vectors parallel and normal to the long molecular axis and show ratios $D_{r_{par}}/D_{r_{perp}}\sim 2$ at 298 K. They can be viewed pictorially as arising from strongly hindered motions, pivoting on the hydrogen bond, that arise as a consequence of strong orientational correlations that extend up to about 8 Å.[8]

The spectral shape of motions comprised within the 10–20 ps region is best seen in the $C_1(\omega)$ Fourier transform of $C_1(t)$ shown in Fig. 5. They give rise to a quasielastic component wider than that arising from the long times and has a shape accountable by a Cole-Davidson function as is also shown in Fig. 5.

A. Rotation-translation coupling

To clarify further the origin of motions having a mixed rotational-translation character we have evaluated the functions $F_{rt}(Q,t)=F_{at}(Q,t)-F_{cm}(Q,t)F_{rot}(Q,t)$ which provide a measure of the extent of rotation-translation coupling (RTC). Here $F_{at}(Q,t)$ stands for the intermediate scattering function calculated as an average over all atoms comprising

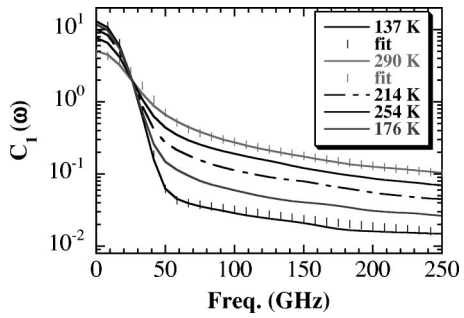

FIG. 5. $C_1(\omega)$ Fourier transforms of $C_1(t)$ into frequency space for temperatures given in the inset. The approximation of such spectra in terms of a Lorentzian plus a Cole-Davidson function are shown for the two extreme temperatures.

a molecule, $F_{cm}(Q,t)$ corresponds to that concerning the molecular centers of mass, and $F_{rot}(Q,t)$ to the rotational part that is evaluated from $C_1(t)$ by means of a conventional partial-wave expansion.[15]

Plots of $F_{rt}(Q,t)$ thus provide an approximate measure of rotation-translation coupling[15] as a function of time, wave vector, and temperature and some examples are shown in Fig. 6. At high temperatures (288 K) RTC barely lasts a few picoseconds and the breadth of $F_{rt}(Q,t)$ increases with increasing wave vector. Such extent of time increases significantly reaching some 100 ps at a temperature well within the normal-liquid range such as 224 K. Again it is seen that its strength increases with Q. This is understood as a consequence of the faster decay of $F_{at}(Q,t)$ which makes the center of $F_{rt}(Q,t)$ to shift towards shorter times with increasing Q values.

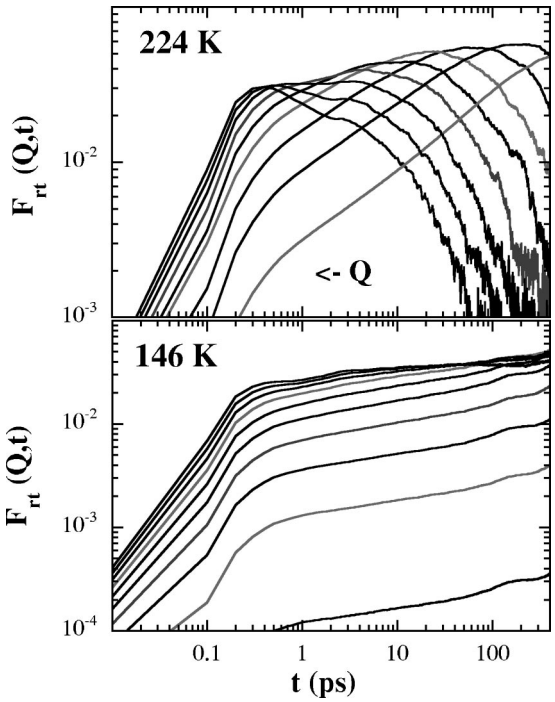

FIG. 6. The Q dependence of the $F_{rt}(Q,t)$ translation-rotation coupling function for Q values spanning from 0.5 $Å^{-1}$ up to 3.3 $Å^{-1}$ from right to left and for temperatures comprising the normal (224 K) and SCL (146 K) liquids.

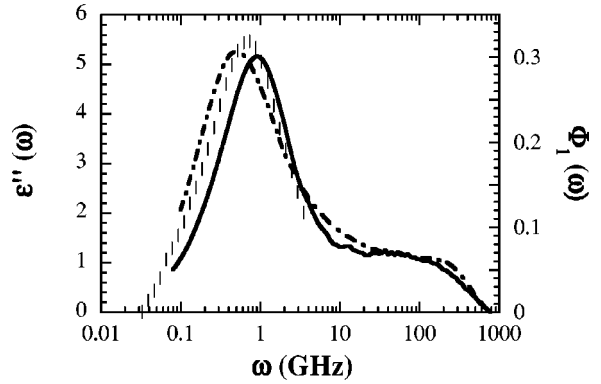

FIG. 7. A comparison of the FL transform of the $\Phi_s(\omega)$ single-dipole quantity (dash-dotted line) to the calculated total dipole function $\epsilon''(\omega)$ (thick line) as calculated for $T=292$ K. The vertical bars display experimental data as measured at $T=288$ K.

For a temperature just below melting, $T=146$ K, the curves shown in Fig. 6 indicate that rotation and translational motions are significantly coupled at most times. Within these temperatures, RTC spans a time region comprising the intermediate- and long-time regimes discussed above in relation with $C_1(t)$. Put into different words, one should expect us to find within the SCL motional features that are not pure rotations or translations. Decoupling of translational diffusion within the SCL will finally result as a consequence of the complete decay of $F_{at}(Q,t)$ and will take place at macroscopic time scales only accessible through dielectric spectroscopy.

B. Calculation of the dielectric response

The transformation of $C_1(t)$ into the frequency domain by means of Fourier-Laplace (FL) transformation yields quantities $\Phi_s(\omega)$ that would correspond to the dielectric spectra of a set of individual dipoles. Such a function is to be compared with the FL transform of the total dipole moment correlation function $\Phi_{coll}=\langle M(0)M(t)\rangle/\langle M^2\rangle$ that would correspond to that measured experimentally. Unfortunately,[10] the statistical accuracy achievable for Φ_{coll} precludes any realistic comparison between this quantity and $C_1(\omega)$ at temperatures within the SCL or even the cold-liquid ranges. Figure 7 displays a comparison between the single-dipole and collective functions corresponding to the two most intense features (i.e., the peak arising from the high-frequency oscillation in $C_1(t)$ is omitted for the sake of clarity).

Both functions exhibit the same basic structure, that is, a strong Lorentzian low-frequency peak and a shoulder (or peak) located about two decades above in frequency with an amplitude one order of magnitude weaker than the main peak. The result compares favorably with the experimental finding and shows that, at those temperatures where orientational correlations last for short times only, the basic structure of $\epsilon(\omega)$ can be well understood on the basis of the reorientation of a single molecular dipole which, contrary to usual assumptions, shows widely different motional time scales.

Figure 8 displays the temperature dependence of the inverse of the frequency corresponding to peak maxima of $\Phi_s(\omega)$ for the whole set of temperatures where the FL transform could be performed with enough accuracy (down to $1.5T_g$). A fit to the VFT equation setting the value of the activation energy to 1510 K, which is given by experiment for the main peak, yielded a value for the effective temperature $T_0\approx 46$ K, which is 8 K below experiment and an attempt frequency of 0.36 THz which also stands a comparison to the experimental estimate (0.17 THz). In other words, down to $1.5T_g$, the maxima of the single-dipole quantity remarkably follow the behavior of the collective relaxation as measured by experiment.

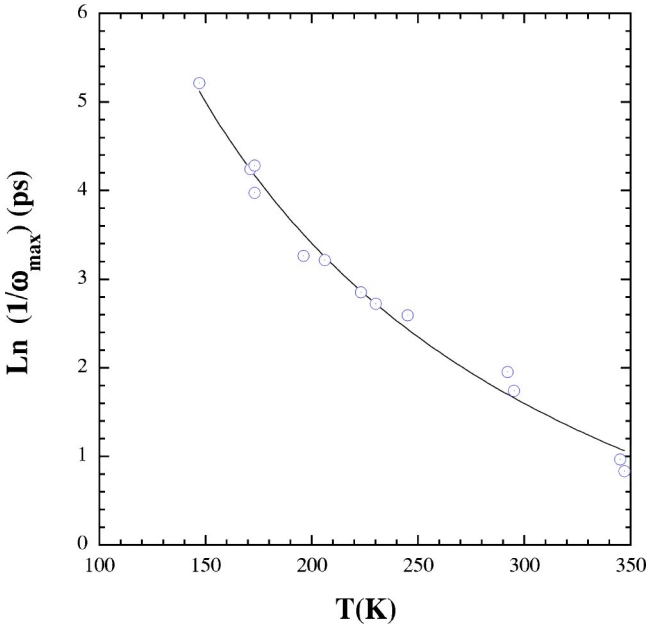

FIG. 8. The temperature dependence of maxima corresponding to the most intense peak in $\Phi_s(\omega)$. The solid line shows a Vogel-Fulcher-Tamann fit made setting the activation energy to the value found experimentally for the α peak.

A point worth remarking at this stage concerns the nature of $\Phi_s(\omega)$. While this is a genuine single-particle quantity, it senses the effects of the collective dynamics in much the same way as a vibrational density of states does. That is, all the dynamics details are projected into this quantity, and therefore it follows the increased hindering to molecular reorientations that accompanies the 2×10^5 increase in value of the shear viscosity.

From data discussed so far we can tentatively establish a relationship between the three time (frequency) regions of $C_1(t(\omega))$ and the three main features of the dielectric spectrum. The strong Debye peak is clearly identifiable with the exponential relaxation appearing at long times and the same applies to the β-relaxation peak that is seen to arise from the fast finite-frequency motions appearing at short times. What is worth emphasizing here is the relationship found between the intermediate-time region of $C_1(t)$ and the Cole-Davidson shoulder appearing in both Φ_{coll} and $\Phi_s(\omega)$.

IV. DISCUSSION

The presence of at least three relaxations with well-separated decay times shown by dielectric spectroscopy is

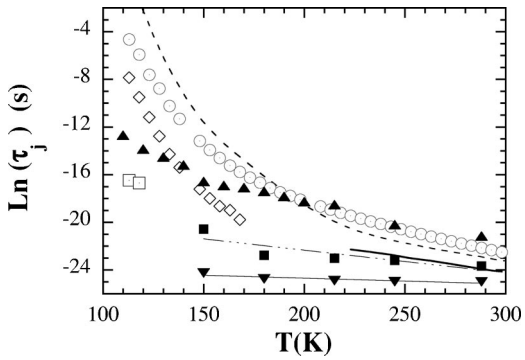

FIG. 9. Characteristic times as derived from the various techniques. Open circles show dielectric data for the main peak. Open lozenges display data for the secondary relaxation (Ref. 3) and open squares correspond to the high-frequency (β) relaxation. QENS data for the narrowest line are given by the black triangles and the two higher-frequency components by black squares and black inverted triangles. The straight lines are exponential fits and serve as guides to the eye. ^{17}O NMR relaxation data as calculated from activation parameters given in Ref. 11 are given by the thick straight line. The characteristic time derived from the macroscopic shear viscosity and a Stokes-Einstein relation is shown by the dotted line.

thus confirmed by our neutron and simulation results. A comparison of the temperature dependence of their characteristic times is provided in Fig. 9. To display equivalent quantities as derived from the different sources, we have first derived from the QENS linewidths and the effective translational diffusion constants referred to above, characteristic times defined as $\tau_{trans}=d_0^2/6D_T$ given by the inverse of the effective self-diffusion coefficients and the molecular diameters d_0.[16] Also, rotational correlation times are derived from QENS data as $\tau_{rot}=1/6D_R$, where D_R are determined after subtraction of the translational components from the measured quasielastic widths.

The experimental dielectric relaxation times are corrected for friction effects following[17]

$$\tau_i=\frac{2\epsilon_\infty+1}{2\epsilon_0+1}\tau_D, \tag{3}$$

where τ_D is the dielectric relaxation time as determined by experiment, and those derived from simulation. The latter correspond to the temperature dependence of the position of the main peak in $\epsilon_{s(\omega)}$ as explained above.

The data displayed in Fig. 9 show that τ_{trans} for temperatures down to $\approx$180 K closely follow the main dielectric relaxation time. As referred to above, the Q dependence of their linewidths and intensities shown in Fig. 2 pinpoints long-range translational diffusion as the main contributor to these line broadenings. This serves to ascribe the origin of the main dielectric peak within this temperature range to the α peak usually identified with liquid flow effects. Within this temperature range, both neutrons, dielectrics, and simulation portray a regime that approaches the Brownian dynamics (Stokes-Einstein, SE) limit. Here one could superimpose data available for the shear viscosity, leaving a mismatch for $T \leqslant 200$ K or the converse as done in Ref. 2. As far as molecular rotations are concerned, data shown in Fig. 9 concerning rotational constants derived from QENS can be satisfactorily compared to those derived from the long-time limits of $C_1(t)$. Their temperature dependence is significantly weaker than that exhibited by translational diffusion, and above 150 K they follow an Arrhenius law. Such low activation energy allows molecular rotations to be thermally activated at temperatures well into the deep SCL phase.

The dielectric data for the secondary relaxation comprises temperatures within the SCL range which also are accessible to QENS. In fact, Fig. 9 shows that both data sets cross each other at $T \approx T_m$. $F_{rt}(Q,t)$ evaluated for $T=146$ K shows that within these temperatures molecular motions have a mixed rotation-translation character and this serves to explain at least on semiquantitative grounds the observed Q dependence of the QENS linewidths. The strong coupling between rotation and translation points towards a strongly cooperative phenomenon, a view in stark contrast with others that portray motions within this frequency range as arising from free molecules.[7] The fact that shear viscosity data display a curvature closer to that of such relaxation than to the main α peak suggests that the motions just referred to are here the main contributors to the viscosity. Although any detailed comparison is limited by the paucity of data concerning the β relaxation, our present data give support to the view of these relaxations as resulting from high-frequency reorientational motions having finite frequencies such as those found in the reorientational functions at short times.

Finally, our results provide an illustration of how Debye-like shapes for the main relaxations may appear within the SCL under conditions of strong translation-rotation coupling where the diffusion approximations break down. The exponential relaxation regime is there attained after a long lapse of time and its appearance is in line with the prediction made in Ref. 18 to explain the observation of Debye shapes in strongly interacting liquids, a fact that puzzled the community since the early days of dielectric spectroscopy.[1]

ACKNOWLEDGMENTS

Work supported in part by Grant No. MAT2002-04540-C05-03 (Spain), the French CNRS, and the U.S. Department of Energy under Contract No. W-31-109-ENG-38. The authors are grateful to the ISIS staff for technical assistance.

[1] H. Frölich, *Theory of Dielectrics* (Oxford Science, Oxford, 1958), p. 88; J. Barthel, K. Bachhuber, R. Buchner, and H. Hetzenauer, Chem. Phys. Lett. **165**, 369 (1990); J.T. Kindt and C.A. Schmuttenmaer, J. Phys. Chem. **100**, 10 373 (1996); S.K. Garg and C.P. Smyth, *ibid.* **69**, 1294 (1965); D.W. Davidson and R.H. Cole, J. Chem. Phys. **18**, 1417 (1951).

[2] C. Hansen, F. Stickel, T. Berger, R. Richert, and E.W. Fischer, J. Chem. Phys. **107**, 1086 (1997).

[3] M. Jiménez-Ruiz *et al.* (unpublished); For additional data see Ref. 2; M.A. Miller, M. Jimenez-Ruiz, F.J. Bermejo, and N.O.

Birge, Phys. Rev. B **57**, R13 977 (1998).
[4] G. Power, G.O. Johari, and J.K. Vij, J. Chem. Phys. **116**, 4192 (2002)
[5] A. Döss, M. Paluch, H. Sillescu, and G. Hinze, Phys. Rev. Lett. **88**, 095701 (2002); S. Hensel-Bielowka and M. Paluch, *ibid.* **89**, 25704 (2002).
[6] R. Brand, P. Lunkenheimer, U. Schneider, and A. Loidl, Phys. Rev. Lett. **82**, 1951 (1999).
[7] S.S.N. Murthy and M. Tyagi, J. Chem. Phys. **117**, 3837 (2002).
[8] C. Talòn, F.J. Bermejo, C. Cabrillo, G.J. Cuello, M.A. Gonzalez, J.W. Richardson, Jr., A. Criado, M.A. Ramos, S. Vieira, F.L. Cumbrera, and L.M. Gonzalez, Phys. Rev. Lett. **88**, 115506 (2002).
[9] C. Talòn, M.A. Ramos, S. Vieira, I. Shmyt'ko, N. Afanisova, A. Criado, G. Madariaga, and F.J. Bermejo, J. Non-Cryst. Solids **287**, 226 (2001); M.A. Ramos, C. Talón, and S. Vieira, *ibid.* **307-310**, 80 (2002).
[10] C. Talòn, G.J. Cuello, M.A. Gonzalez, F.J. Bermejo, C. Cabrillo, and R. Connatser, Chem. Phys. **292**, 263 (2003). For details concerning simulations on related materials, see M.A. González, E. Enciso, F.J. Bermejo, and M. Bée, Phys. Rev. B **61**, 6654 (2000); Phys. Rev. E **61**, 3884 (2000). Preliminary simulation data for the supercooled liquid are given in M.A. González, E. Enciso, F.J. Bermejo, and C. Cabrillo, Philos. Mag. A (to be published).
[11] H. Versmold, Ber. Bunsenges. Phys. Chem. **78**, 1318 (1974); Z. Zheng, C.L. Mayne, and D.M. Grant, J. Magn. Reson. **103**, 268 (1992); S. Meckl and M.D. Zeidler, Mol. Phys. **63**, 85 (1988); R. Ludwig, M.D. Zeidler, and T.C. Farrar, Z. Phys. Chem. (Munich) **189**, 19 (1995); N. Karger, T. Vardag, and H.D. Lüdemann, J. Chem. Phys. **93**, 3437 (1990).
[12] D.S. Sivia and C.J. Carlile, J. Chem. Phys. **96**, 170 (1992). See also D.S. Sivia, *Data Analysis, A Bayesian Tutorial* (Oxford University Press, Oxford, 1996).
[13] W.G. Rothschild, J. Soussen-Jacob, J. Bessiere, and J. Vincent-Geise, J. Chem. Phys. **79**, 3002 (1983).
[14] R. Hilfer, Phys. Rev. E **65**, 061510 (2002).
[15] S.H. Chen, P. Gallo, F. Sciortino, and P. Tartaglia, Phys. Rev. E **56**, 4231 (1997).
[16] J.M. McConell, *The Theory of Nuclear Magnetic Relaxation in Liquids* (Cambdridge University Press, Cambridge, 1987), p. 76.
[17] J.B. Hubbard and P.G. Wolynes, J. Chem. Phys. **69**, 998 (1978).
[18] B. Bagchi and A. Chandra, Phys. Rev. Lett. **64**, 455 (1990).